Title

Switching of the folding-energy landscape governs the allosteric activation of protein kinase A

Journal

Proceedings of the National Academy of Sciences of the United States of America, 115(32)

ISSN

0027-8424

Authors

England, Jeneffer P
Hao, Yuxin
Bai, Lihui
et al.

Publication Date

2018-08-07

DOI

10.1073/pnas.1802510115

Peer reviewed

Switching of the folding-energy landscape governs the allosteric activation of protein kinase A

Jeneffer P. England[a], Yuxin Hao[a], Lihui Bai[a], Virginia Glick[a], H. Courtney Hodges[b,c,d,e], Susan S. Taylor[f,g,1], and Rodrigo A. Maillard[a,1]

[a]Department of Chemistry, Georgetown University, Washington, DC 20057; [b]Department of Molecular and Cellular Biology, Baylor College of Medicine, Houston, TX 77030; [c]Center for Precision Environmental Health, Baylor College of Medicine, Houston, TX 77030; [d]Dan L Duncan Comprehensive Cancer Center, Baylor College of Medicine, Houston, TX 77030; [e]Center for Cancer Epigenetics, The University of Texas MD Anderson Cancer Center, Houston, TX 77030; [f]Department of Pharmacology, University of California, San Diego, La Jolla, CA 92093; and [g]Department of Chemistry and Biochemistry, University of California, San Diego, La Jolla, CA 92093

Contributed by Susan S. Taylor, June 29, 2018 (sent for review February 13, 2018; reviewed by Ruben L. Gonzalez Jr., Taekjip Ha, and Keir C. Neuman)

Protein kinases are dynamic molecular switches that sample multiple conformational states. The regulatory subunit of PKA harbors two cAMP-binding domains [cyclic nucleotide-binding (CNB) domains] that oscillate between inactive and active conformations dependent on cAMP binding. The cooperative binding of cAMP to the CNB domains activates an allosteric interaction network that enables PKA to progress from the inactive to active conformation, unleashing the activity of the catalytic subunit. Despite its importance in the regulation of many biological processes, the molecular mechanism responsible for the observed cooperativity during the activation of PKA remains unclear. Here, we use optical tweezers to probe the folding cooperativity and energetics of domain communication between the cAMP-binding domains in the apo state and bound to the catalytic subunit. Our study provides direct evidence of a switch in the folding-energy landscape of the two CNB domains from energetically independent in the apo state to highly cooperative and energetically coupled in the presence of the catalytic subunit. Moreover, we show that destabilizing mutational effects in one CNB domain efficiently propagate to the other and decrease the folding cooperativity between them. Taken together, our results provide a thermodynamic foundation for the conformational plasticity that enables protein kinases to adapt and respond to signaling molecules.

kinase | cAMP | optical tweezers | allostery | single molecule

Protein kinases play a major role in the regulation of most biological processes in eukaryotes, including cell growth and development, metabolism, and signaling (1). These biological processes have been associated with numerous human diseases and have led to the emergence of kinases as major therapeutic drug targets (2, 3). A well-characterized member of the kinase family is PKA, a ubiquitous cAMP-responsive eukaryotic kinase that modulates protein function through targeted phosphorylation (4, 5).

In the cell, PKA exists as a heterotetramer composed of a dimeric regulatory subunit and two monomeric catalytic subunits. The catalytic subunit has a small and a large lobe that form an active site cleft (Fig. 1*A*). The regulatory subunit is composed of an N-terminal flexible linker domain that contains the dimerization domain (D/D), an inhibitory sequence (IS), and two cyclic nucleotide-binding (CNB) domains, CNB-A and CNB-B, that are connected by an extended α-helix known as the "αB/C helix" (Fig. 1 *A* and *B*, shown in maroon) (4, 6).

Biochemical, structural, and biophysical studies have shown that a PKA heterodimer (Fig. 1*B*, *Left*) composed of a single catalytic and regulatory subunit displays functional cooperativity and therefore is a significant component of the inactive heterotetrameric complex (4, 5, 7–9). The crystal structure of the inactive PKA heterodimer solved by Kim et al. (4) shows that the regulatory subunit is bound to the catalytic subunit via surface interactions and through docking of the inhibitory sequence (shown in orange in Fig. 1 *A* and *B*) into the active site of the catalytic subunit. The surface interactions between the catalytic subunit and the regulatory subunit are mediated predominately by the N3A motif of the CNB-A domain (shown in teal in Fig. 1 *A* and *B*) and the αB/C helix (shown in maroon in Fig. 1 *A* and *B*). In addition, the end of the αB/C helix provides most of the interaction surface between the CNB-B domain and the catalytic subunit.

Biochemical and mutational studies have shown that the activation of the PKA heterodimer starts with cAMP binding to the CNB-B domain (4, 6, 10). This first binding event allosterically triggers the cooperative binding of a second cAMP molecule to the CNB-A domain, resulting in a large conformational change in the regulatory subunit (Fig. 1*B*, *Right*). The structure of the PKA heterodimer shows that the catalytic subunit blocks the cAMP-binding pocket of the CNB-A domain, while the pocket in the CNB-B domain remains solvent accessible. Although these structural data provide evidence for the role of the CNB-B domain as the gatekeeper for the cAMP-dependent activation of PKA (4, 6), the molecular mechanism and thermodynamic driving forces responsible for the allosteric communication between CNB domains still remain unknown (7, 11, 12). To address this long-standing question, we use single-molecule optical tweezers (13–16) to selectively probe the folding cooperativity and extract the energetics of domain communication between the CNB domains in the apo state and bound to the catalytic subunit.

The results from this study show that the CNB domains in the apo state behave as energetically independent structural

Significance

Mutations, deletions, or gene fusions in protein kinases have been associated with the development of many diseases in humans and have led to the emergence of the protein kinase family as an important therapeutic drug target. In the cell, kinase activity is often turned on and off allosterically by intramolecular regulatory domains, flexible linkers, or other interacting proteins. Here, we use single-molecule optical tweezers to investigate the mechanism of allosteric regulation of the cAMP-dependent PKA. This approach allowed us to determine the thermodynamic driving forces that enable PKA to transduce cAMP-binding signals to turn on its kinase activity.

Author contributions: J.P.E., S.S.T., and R.A.M. designed research; J.P.E., L.B., and V.G. performed research; Y.H. and L.B. contributed new reagents/analytic tools; J.P.E., Y.H., L.B., H.C.H., and R.A.M. analyzed data; and J.P.E., Y.H., H.C.H., S.S.T., and R.A.M. wrote the paper.

Reviewers: R.L.G., Columbia University; T.H., Johns Hopkins University; and K.C.N., National Heart, Lung, and Blood Institute, National Institutes of Health.

The authors declare no conflict of interest.

[1]To whom correspondence may be addressed. Email: staylor@ucsd.edu or rodrigo.maillard@georgetown.edu.

This article contains supporting information online at www.pnas.org/lookup/suppl/doi:10.1073/pnas.1802510115/-/DCSupplemental.

Published online July 23, 2018.

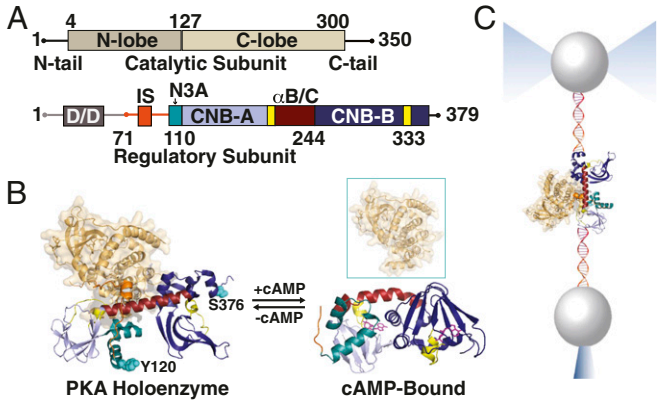

Fig. 1. Structure, domain organization, and optical tweezers assay to study PKA. (*A*) Domain organization of PKA. The catalytic subunit has an N- and a C-lobe that form an active-site cleft. The regulatory subunit has a modular domain organization. The D/D (shown in grey) and the flexible linker domain (residues 71–110, shown in orange) contain the IS that mimics the peptide substrate of the catalytic subunit. Two CNB domains, CNB-A (light purple) and CNB-B (dark purple), are connected by the αB/C helix (maroon). The N3A motif of the CNB-A domain is shown in teal. The cAMP-binding pocket of each CNB domain is shown in yellow. (*B*, *Left*) The PKA complex is shown in the inactive form in which the catalytic subunit (tan) is bound to the regulatory subunit (light and dark purple). (*Right*) The binding of two molecules of cAMP results in a conformational change in the regulatory subunit (cAMP-bound form) and enables the release of the active catalytic subunit (boxed in green). (*C*) Optical tweezers experimental set-up. The regulatory subunit is tethered between two polystyrene beads by the attachment of DNA handles at positions flanking the CNB domains (Y120/S376) shown in cyan in *B*). The PKA complex is formed *in trans* with the catalytic subunit, ATP, and Mg^{2+} present in the microfluidic chamber.

elements. However, in the presence of the catalytic subunit the CNB domains have strong cooperative interactions, are more stable, and are in equilibrium between two conformations. The cooperative behavior between CNB domains bound to the catalytic subunit was quantified thermodynamically and revealed a switch in the folding-energy landscape between the apo and bound conformations. The energy landscape in the bound conformation shows that the CNB-B domain serves as an energetic hub, controlling the magnitude of interaction between the CNB-A domain and the catalytic subunit. This result provides a thermodynamic foundation for the gatekeeper function of the CNB-B domain. Last, we demonstrate how destabilizing mutational effects in the CNB-B domain are propagated to the CNB-A domain, causing significant decoupling between the two domains when bound to the catalytic subunit. Taken together, our study provides direct experimental evidence for a thermodynamic switching mechanism in the activation of a protein kinase complex.

Results

Assembly of the PKA Complex in the Optical Tweezers. We used single-molecule optical tweezers (17–19) to study the folding cooperativity between the CNB domains in the apo state or bound to the catalytic subunit. In this assay, a monomeric, cysteine-modified regulatory subunit that lacks the dimerization domain (residues 71–379 of the full-length RIα isoform) (20) was tethered between two beads using two 370-bp DNA handles (Fig. 1*C*). The handles were attached via disulfide bond linkages at positions immediately flanking the two CNB domains (pulling axis Y120/S376 shown in cyan in Fig. 1*B*). This experimental design enabled us to manipulate the CNB domains selectively without directly perturbing other structural elements in the regulatory subunit, such as the N-terminal linker domain, the inhibitory sequence, or the catalytic subunit in PKA. To assemble the PKA heterodimer in the optical tweezers, we tethered a single regulatory subunit and added *in trans* saturating amounts of the catalytic subunit [100 nM in the chamber, $K_d = 0.9$ nm for the assembly of the PKA heterotetramer (21)], ATP, and Mg^{2+} [0.2 mM and 1 mM, respectively, in the chamber, $K_d = 39$ nM (22)]. We collected force–extension curves by moving the bead in the optical trap away from and toward the bead fixed on the micropipette using a constant pulling velocity of 75 nm/s at a 500-Hz sampling rate. Control experiments in bulk were performed to ensure that the DNA handles cross-linked to the regulatory subunit did not affect its interaction with the catalytic subunit (i.e., formation of an inactive PKA heterodimer) or the cAMP-dependent activation mechanism (*SI Appendix*, Fig. S1).

Mechanical Unfolding of the Regulatory Subunit in the Apo State. In the apo state, the force–extension curves revealed two consecutive unfolding transitions, or rips, that correspond to the mechanical denaturation of the CNB domains (Fig. 2*A*, *Left*). The first rip had a change in contour length (ΔLc) of 50.3 ± 0.1 nm (mean ± SE, $n = 452$) and a mean unfolding force of 9.1 ± 0.1 pN (Table 1). These values are very similar to those obtained for the truncated CNB-B domain (*SI Appendix*, Fig. S2 *A* and *C*). The second rip had a shorter ΔLc of 44.2 ± 0.1 nm occurring at a statistically higher force of 10.5 ± 0.1 pN (kstest2, $P < 0.01$) that matched the values obtained for the truncated CNB-A domain (*SI Appendix*, Fig. S2 *B* and *C*). The agreement between the truncated CNB domains and the first and second rip suggest that the CNB domains in the regulatory subunit behave as independent structures. Interestingly, despite the small difference in mean unfolding force between the two CNB domains, we observed a strong bias in the unfolding pathway: The CNB-B unfolds first in ∼90% of all trajectories, followed by the CNB-A domain (*SI Appendix*, Fig. S2 *D–F*).

To assess whether our mechanical unfolding observations of the regulatory subunit in the apo state were consistent with independent and sequential unfolding events, we performed discrete time Monte Carlo simulations (*SI Appendix*, *Section 1.11* and Fig. S3 *A–D*). Briefly, the CNB domains were treated as worm-like chains that were covalently linked in series and tethered by 740 bp of total DNA handles (similar to our experimental conditions). We used the kinetic parameters obtained from unfolding force distributions for the apo CNB-A and CNB-B domains shown in Table 1 to simulate individual force–extension curves. In agreement with our experimental unfolding curves, simulations revealed a two-step unfolding event representing the mechanical unfolding of the CNB domains (*SI Appendix*, Fig. S3*A*), in which the CNB-B unfolded first in ∼87% of the total trajectories ($n = 2{,}000$) (*SI Appendix*, Fig. S3*B*) and at a mean unfolding force of 8.5 pN (*SI Appendix*, Fig. S3*C*). The CNB-A domain unfolded at a slightly higher average force of 11 pN (*SI Appendix*, Fig. S3*C*). We therefore conclude that in the apo conformation the two CNB domains behave as mechanically independent domains that unfold in a sequential fashion so that the CNB-B domain unfolds first (rip 1) followed by the CNB-A domain (rip 2).

Selective Force-Induced Denaturation of the Regulatory Subunit Bound to the Catalytic Subunit. In the presence of the catalytic subunit, the single-molecule trajectories of the CNB domains revealed two clearly distinct unfolding pathways, labeled "I" and "II" (Fig. 2*A*, *Center* and *Right*, $n = 1{,}041$). In unfolding pathway I we observed two unfolding rips that occurred almost simultaneously and at forces higher than those seen in the apo state. The simultaneous unfolding behavior of the CNB domains suggests that the fold of these domains is highly cooperative when bound to the catalytic subunit. The higher unfolding forces indicate that both CNB domains establish significant surface interactions with the catalytic subunit. For instance, the CNB-A domain experiences an increase in its mean unfolding force from 10.5 ± 0.1 pN in the apo state to 13.6 ± 0.1 pN when bound to the catalytic

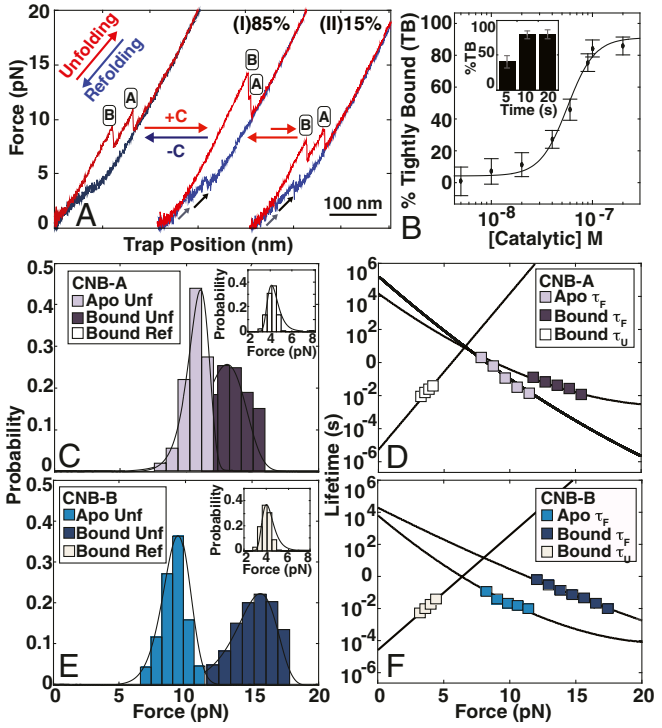

Fig. 2. Mechanical unfolding of the wild-type regulatory subunit. (*A*) Representative force–extension curves for the mechanical unfolding of the regulatory subunit (residues 71–379) in the absence (*Left*) and presence (*Right*) of the catalytic subunit. In the absence of the catalytic subunit, only one unfolding pathway is observed with two rips. In the presence of the catalytic subunit, two unfolding pathways, I and II, are observed that correspond to different conformations of the regulatory subunit. (*B*) Titration of the catalytic subunit increases the percentage of unfolding pathway I [labeled "% Tightly Bound" (TB)]. Saturation occurs at 100 nM catalytic subunit. (*Inset*) The same percentage of unfolding pathway I is observed at 100 nM catalytic subunit with 10-s and 20-s refolding times at 1 pN. (*C*) Unfolding (Unf) and refolding (Ref) force probability distributions for the CNB-A domain are shown for the apo state and bound conformations (light and dark purple bars, respectively). An increase in the unfolding force of 3 pN is observed in the presence of the catalytic subunit. (*Inset*) Refolding force probability distribution in the presence of the catalytic subunit (white bars). (*D*) Folded-state lifetimes (τ_0) as a function of force for the CNB-A domain in the absence and presence of the catalytic subunit (light and dark purple squares, respectively). White squares show the unfolded-state lifetimes (τ_U) as a function of force for the CNB-A domain in the presence of the catalytic subunit. (*E*) Unfolding and refolding force probability distributions for the CNB-B domain in the apo state and bound conformations (light and dark blue bars, respectively). The presence of the catalytic subunit stabilizes the CNB-B domain by ∼6 pN. (*Inset*) Refolding force probability distribution in the presence of the catalytic subunit. (*F*) Folded-state lifetimes (τ_F) as a function of force for the CNB-B domain in the absence and presence of the catalytic subunit (light and dark blue squares, respectively). Light yellow squares show the unfolded-state lifetimes (τ_U) as a function of force for the CNB-A domain in the presence of the catalytic subunit. The lines in *D* and *F* correspond to the best fit of *SI Appendix*, Eq. **S2**, and the lines in *C* and *E* correspond to the best fit of *SI Appendix*, Eq. **S3** (*SI Appendix, Section 1.7*).

subunit. Similarly, the CNB-B domain required a greater unfolding force of 15.2 ± 0.1 pN when bound to the catalytic subunit compared with 9.1 ± 0.1 pN in the apo state (Table 1). In contrast to a highly cooperative unfolding trajectory, unfolding pathway II resembles the apo state: The two CNB domains unfold independently of each other and at forces comparable to the apo state (Fig. 2*A*), which indicates fewer surface interactions with the catalytic subunit.

In addition to the effects seen in the unfolding trajectories, the presence of the catalytic subunit exhibited clear refolding transitions at ∼4 pN for each CNB domain (Fig. 2*A*, *Center* and *Right*, black and gray arrows). The probability of observing refolding transitions for both pathways I and II increased from <1% in the apo state to ∼30% in the presence of the catalytic subunit. It is possible that events corresponding to unfolding pathway II with no detected refolding transitions may correspond to an apo state or to events where refolding transitions are missed due to noise occurring at low forces. Nonetheless, the higher probability of observing the refolding transition suggests that the catalytic subunit not only stabilizes the two CNB domains in the folded state but also, after the protein unfolds the same or another catalytic subunit, may assist in the refolding process of the protein.

Mechanism of Unfolding of the Regulatory Subunit Bound to the Catalytic Subunit. Analyses of the changes in contour length reveal that for both unfolding pathways I and II the CNB-B domain unfolds first, followed by the CNB-A domain (n = *485*) (*SI Appendix*, Fig. S2 *G–I*). We corroborated the domain assignment experimentally by making a regulatory subunit construct with DNA handles attached at position D149 and S379. This construct is fully folded, binds cAMP similarly to wild-type protein, and forms a stable inactive PKA heterodimer (*SI Appendix*, Fig. S4). However, the new pulling position from residue D149 resulted in a significantly shorter change in contour length (ΔLc) upon unfolding for the CNB-A domain [calculated ΔLc = 34 nm from the worm-like chain model (23)], thereby making it easier to distinguish it from the CNB-B domain (calculated ΔLc = 50 nm).

In the presence of the catalytic subunit, the D149/S376 protein construct displayed two clearly distinct unfolding rips, the first with a ΔLc of ∼50 nm and the second with a ΔLc of ∼34 nm, indicating that the CNB-B unfolded first followed by CNB-A (*SI Appendix*, Fig. S4 *A* and *B*). Moreover, the distribution of unfolding forces and the ΔLc upon unfolding of the CNB-B domain in D149/S376 were indistinguishable from those seen in the first rip in the Y120/S376 protein (*SI Appendix*, Fig. S5). These results directly confirm that, in the presence of the catalytic subunit and independent of unfolding pathways I and II, the CNB-B domain unfolds first, followed by the CNB-A domain.

The Ensemble of the Inactive PKA Complex Comprises Tightly and Loosely Bound Conformations. The presence of unfolding pathways I and II suggests a scenario in which the regulatory subunit bound to the catalytic subunit is in equilibrium between two conformations. An alternative scenario is that the two unfolding pathways result from specific experimental conditions used in the assay. For example, different unfolding pathways may result (*i*) from having the regulatory subunit unbound (apo state) or sometimes bound to the catalytic subunit (i.e., if the catalytic subunit concentration is lower than the K_d of heterodimer formation) a fraction of the time and (*ii*) from not allowing sufficient time for the regulatory subunit to refold and rebind the catalytic subunit before the next unfolding cycle.

To discriminate between these two scenarios, we titrated increasing amounts of the catalytic subunit from 5 nM to 200 nM and increased the refolding and rebinding time from 5 s to 20 s. Fig. 2*B* shows that as we increased the concentration of the catalytic subunit, the percentage of events displaying highly cooperative unfolding rips (unfolding pathway I) increased in a sigmoidal fashion resembling a ligand titration curve with a K_d of ∼40 nM. When the catalytic subunit concentration was ≥80 nM, the percentage of events corresponding to unfolding pathway I plateaued at ∼85%. The other ∼15% of events corresponded to unfolding pathway II in which the CNB domains unfold independently of each other. The same percentages were observed when the time to refold and rebind was increased from 10 s to 20 s using 100 nM of catalytic subunit (Fig. 2*B*, *Inset*). In contrast, a decrease from 10 s to 5 s resulted in 43% unfolding pathway I,

Table 1. Kinetic and thermodynamic parameters for each CNB domain in the PKA regulatory subunit

	Wild-type Apo		Wild-type bound		R333K bound	
Parameters	CNB-A	CNB-B	CNB-A	CNB-B	CNB-A	CNB-B
F_{mean}, pN	10.5 ± 0.06	9.1 ± 0.06	13.6 ± 0.04	15.2 ± 0.04	10.5 ± 0.04	11.5 ± 0.04
$\tau_{0,F}$, s	6.0 ± 0.4 × 10^5	1.0 ± 0.2 × 10^4	1.0 ± 0.1 × 10^4	4.6 ± 0.1 × 10^4	2.8 ± 1.0 × 10^4	5.0 ± 0.3 × 10^4
$\Delta x^{\ddagger}_{F\to U}$, nm	6.4 ± 0.1	6.0 ± 0.1	4.2 ± 0.1	3.7 ± 0.1	5.8 ± 0.2	6.7 ± 0.1
$\tau_{0,U}$, s	N.d.	N.d.	2.0 ± 0.9 × 10^{-5}	4.0 ± 1.3 × 10^{-5}	N.d.	2.0 ± 1.0 × 10^{-4}
$\Delta x^{\ddagger}_{U\to F}$, nm	N.d.	N.d.	8.6 ± 0.4	8.2 ± 0.4	N.d.	7.0 ± 0.4
$\Delta G^{\ddagger}_{F\to U}$, k_BT	36.6 ± 1.6	20.9 ± 1.4	18.4 ± 2.9	33.7 ± 0.6	20.5 ± 2.2	23.9 ± 0.4
ΔG^{0}, kcal/mol	5.8 ± 0.7*	5.7 ± 2.9*	11.9	12.4	N.d.	11.0
	3.8 ± 0.3†	2.8 ± 1.0†				

N.d., not determined.
*CD unfolding data.
†Tryptophan fluorescence unfolding data.

35% unfolding pathway II, and 22% of events showing only one domain refolding or no refolding at all.

Based on these results, we conclude that the two unfolding pathways I and II are not due to specific experimental conditions but reflect two conformational states of the inactive ensemble of PKA. In unfolding pathway I the CNB domains unfold in a highly cooperative fashion and at high forces, indicating that both CNB domains are tightly bound to the catalytic subunit. In contrast, in unfolding pathway II we observed the CNB domains unfolding independently and at forces similar to those seen in apo-unfolding trajectories, suggesting that the CNB domains are loosely bound to the catalytic subunit.

The Energy Landscape Describes the Cooperative Behavior of the CNB Domains Bound to the Catalytic Subunit. The data corresponding to unfolding pathway I allowed us to dissect the thermodynamic driving forces underlying the cooperative behavior of the CNB domains tightly bound to the catalytic subunit. Specifically, we transformed the unfolding force probability distributions of each CNB domain into lifetimes as a function of force (24, 25) to extract the folded state lifetime ($\tau_{0,F}$), distance to the transition state ($\Delta x^{\ddagger}_{F\to U}$), and energy barrier ($\Delta G^{\ddagger}_{F\to U}$) at zero force (Fig. 2 *C–F* and Table 1).

For the CNB-A domain, $\tau_{0,F}$ was larger and $\Delta x^{\ddagger}_{F\to U}$ was longer in the apo state than in the tightly bound conformation. For the CNB-B domain in the apo state, $\tau_{0,F}$ was shorter and $\Delta x^{\ddagger}_{F\to U}$ was longer than in the tightly bound conformation. Compared with other folded proteins studied under force (17, 26–30), both CNB domains in the apo state had an unusually large $\Delta x^{\ddagger}_{F\to U}$. A similar $\Delta x^{\ddagger}_{F\to U}$ was reported for apomyoglobin, a molten globule-like protein that lacks well-packed tertiary interactions at low pH (31). Thus, in the absence of the catalytic subunit the regulatory subunit is compliant and deformable. In contrast, both CNB domains bound to the catalytic subunit experienced a significant reduction in $\Delta x^{\ddagger}_{F\to U}$, suggesting that these domains become more brittle, or less flexible, when they are bound to the catalytic subunit.

A similar analysis of the refolding force probability distributions in the presence of the catalytic subunit (Fig. 2 *C* and *E*, *Insets* and *SI Appendix*, Fig. S6) enabled us to extract the unfolded state lifetimes at zero force ($\tau_{0,U}$) and the distance to the transition state for the refolding reaction ($\Delta x^{\ddagger}_{U\to F}$) (Fig. 2 *D* and *F*). Both CNB domains exhibited similar $\tau_{0,U}$ and $\Delta x^{\ddagger}_{U\to F}$ when tightly bound to the catalytic subunit: The CNB-A domain had a $\tau_{0,U} = 2.0 \times 10^{-5}$ s and a $\Delta x^{\ddagger}_{U\to F} = 8.6$ nm, whereas the CNB-B domain had a $\tau_{0,U} = 4.0 \times 10^{-5}$ s and a $\Delta x^{\ddagger}_{U\to F} = 8.2$ nm.

Having obtained the lifetimes of the folded and unfolded states at zero force, we estimated the equilibrium free energy of unfolding for each CNB domain bound to the catalytic subunit using $\Delta G^{0}_{bound} = -RT \cdot ln[\tau_{0,U}/\tau_{0,F}]$, where $RT = 0.592$ kcal/mol. We obtained $\Delta G^{0}_{bound} = 12.9$ kcal/mol for the CNB-A domain and $\Delta G^{0}_{bound} = 12.1$ kcal/mol for the CNB-B domain. Since refolding transitions of the CNB domains were rarely detected in the absence of the catalytic subunit, we performed bulk urea denaturation experiments monitored by CD (*SI Appendix*, Fig. S7 *A–D*) and tryptophan fluorescence (*SI Appendix*, Fig. S7 *E–H*) to estimate the unfolding free energy of each CNB domain in the apo state (ΔG^{0}_{apo}). We obtained a ΔG^{0}_{apo} value of ∼5.8 kcal/mol for the CNB domains using CD, which reflects the global stability of the secondary structures of the domains. The stability values were slightly lower when monitored by changes in tryptophan fluorescence. These results indicate that the local environment surrounding the tryptophan residues is less stable than the global fold of the protein (*SI Appendix*, Table S1). Independent of the technique used to measure the stability of the CNB domains in the apo state, there is a substantial thermodynamic stabilization effect (8.5–10 kcal/mol) of the CNB domains when they are tightly interacting with the catalytic subunit. This stabilization or coupling energy provides a thermodynamic foundation for the cooperative unfolding behavior of the two CNB domains.

Another important difference between the apo state and the tightly bound conformation is reflected in the height of the energy barrier, $\Delta G^{\ddagger}_{F\to U}$. Unfolding the CNB-A domain in the apo state required a $\Delta G^{\ddagger}_{F\to U} = 36.6$ k_BT [where the Boltzmann constant (k_B) at 298 K (T) is equal to 4.114 pN × nm], whereas when bound to the catalytic subunit it required a $\Delta G^{\ddagger}_{F\to U} = 18.4$ k_BT. The opposite trend is observed for the CNB-B domain, requiring a $\Delta G^{\ddagger}_{F\to U} = 20.9$ k_BT in the apo state and 33.7 k_BT when bound to the catalytic subunit (Table 1). Interestingly, while the CNB domains unfold following the same reaction order in our experiments, the protein has very different underlying energy landscapes in the presence versus the absence of the catalytic subunit. This difference is reflected by the change in $\Delta G^{\ddagger}_{F\to U}$ and represents a direct measurement of an energetic switch mechanism for a protein-signaling complex, and likely reflects the directionality of the observed functional cooperativity from the CNB-B domain to the CNB-A (B-to-A direction) in the PKA complex (8, 9).

A Single Mutation Breaks the Folding Cooperativity Between the CNB Domains Bound to the Catalytic Subunit. The strong folding cooperativity observed in the B-to-A direction predicts that, when bound to the catalytic subunit, an energetic perturbation in the CNB-B domain will propagate to the CNB-A domain. To test this prediction, we made the mutation R333K in the cAMP-binding pocket of the CNB-B domain and evaluated its long-range effect on the mechanical stability of the CNB-A domain as well as its effect on the folding cooperativity between CNB domains. Previous studies have shown that this mutation does not affect the affinity for the catalytic subunit (7, 9), but it destabilizes the regulatory subunit in the cAMP-bound state (32) and increases both the K_d for cAMP binding and the K_a for cAMP-mediated activation of PKA (9). However, the mechanism by

which a mutational perturbation propagates from one CNB domain to another in the PKA complex remains unknown.

The R333K mutant protein in the apo state had severe folding defects. In the force–extension curve shown in Fig. 3*A*, *Left*, only one fully folded domain is observed in the apo state (measured $\Delta Lc = 44$ nm, $n = 302$), which likely corresponds to the CNB-A domain. In contrast, in the presence of the catalytic subunit the R333K mutant protein showed complete folding of both CNB domains with a high probability of refolding (~73%) (Fig. 3*A*, *Right*), which is in agreement with and corroborates the role of the catalytic subunit in assisting the refolding process seen for the wild-type regulatory subunit. Similar to the wild-type protein,

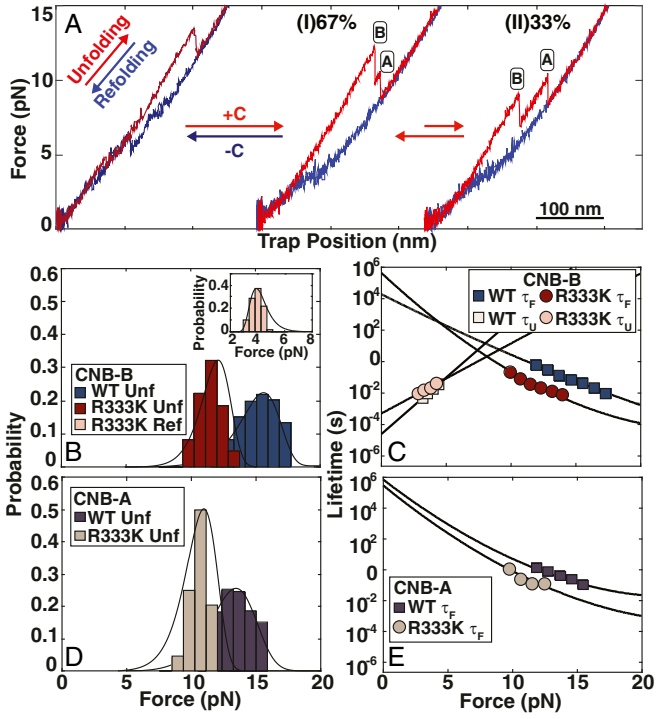

Fig. 3. Mechanical unfolding of the R333K regulatory subunit. (*A*) Representative force–extension curves for the mechanical unfolding of the R333K mutant regulatory subunit in the absence and presence of the catalytic subunit. In the absence of the catalytic subunit, or apo state, we observed two unfolding rips at 5 pN and 13 pN. The rip occurring at 13 pN has a change in extension that is comparable to the CNB-A domain. In contrast, the rip seen at 5 pN has a much lower extension change than that of the CNB-B domain, indicating that this mutant protein in the apo state is partially folded. Incubation with the catalytic subunit facilitates and recovers the correct folding of the R333K mutant regulatory subunit. Unfolding occurs in two unfolding pathways, I and II, a behavior similar to the wild-type construct. (*B*) Unfolding (Unf) force probability distributions for the R333K mutant and wild-type CNB-B domain bound to the catalytic subunit (dark red and dark blue bars, respectively). (*Inset*) Refolding (Ref) force probability distribution of the R333K mutant CNB-B domain in the presence of the catalytic subunit (light orange bars). (*C*) Lifetimes (τ0) as a function of force for the CNB-B domain in the presence of the catalytic subunit. Light orange and dark red spheres correspond to unfolded (τU) and folded-state (τF) lifetimes for the R333K mutant. Light yellow and dark blue squares correspond to unfolded and folded state lifetimes for the wild-type protein. (*D*) Unfolding (Unf) force probability distributions for the R333K mutant and wild-type CNB-A domain bound to the catalytic subunit (light brown and dark purple bars, respectively). No refolding transitions were observed for the R333K mutant CNB-A domain in the presence of the catalytic subunit. (*E*) Folded-state lifetimes (τF) as a function of force for the R333K mutant and wild-type CNB-A domain in the absence and presence of the catalytic subunit (light brown spheres and dark purple squares, respectively). The lines in *C* and *E* correspond to the best fit of *SI Appendix*, Eq. **S2**, and the lines in *B* and *D* correspond to the best fit of *SI Appendix*, Eq. **S3** (*SI Appendix*, *Section 1.7*).

the R333K mutant protein displayed a highly cooperative unfolding pathway (unfolding pathway I) and an apo-like unfolding pathway (unfolding pathway II). However, there were important differences between the wild-type protein and the R333K mutant protein. First, a decrease in the percentage of cooperative unfolding pathway (from 85 to 67%) and an increase in the apo-like unfolding pathway (from 15 to 33%) was observed in the R333K mutant protein (Fig. 3*A*). Second, the unfolding force probability distribution of the mutant CNB-B domain showed lower unfolding forces than in the wild-type protein (~11.5 pN and ~15.2 pN, respectively) (Fig. 3*B*). Unexpectedly, we also measured a lower mean unfolding force for the CNB-A domain in the mutant relative to the wild-type protein (~10.5 pN and ~13.6 pN, respectively) (Fig. 3*D*), a result that directly measures the long-range destabilizing effect of the mutation in the CNB-B domain.

We extracted $\tau_{0,F}$, $\Delta x^{\ddagger}_{F\to U}$, and $\Delta G^{\ddagger}_{F\to U}$ from the unfolding force probability distributions of each CNB domain in the R333K mutant protein and compared the values with those obtained for the wild-type protein (Fig. 3 *C* and *E* and Table 1). For both CNB domains, there were no significant differences in $\tau_{0,F}$ between the mutant and wild-type proteins. However, $\Delta x^{\ddagger}_{F\to U}$ was significantly longer for the R333K mutant protein. A longer $\Delta x^{\ddagger}_{F\to U}$ indicates that the mutant protein exists in a molten globule-like conformation even when it is bound to the catalytic subunit. Analysis of refolding force distributions was possible only for the CNB-B domain, allowing us to determine $\tau_{0,U}$ and $\Delta x^{\ddagger}_{U\to F}$ (Table 1) and $\Delta G^{0}_{bound} = 11$ kcal/mol. As seen for the wild-type protein, the stability of the mutant CNB-B domain due to interactions with the catalytic subunit is ~8.5 kcal/mol higher than the value obtained for the apo state from bulk measurements (*SI Appendix*, Table S1).

The analysis of the unfolding-energy barrier ($\Delta G^{\ddagger}_{F\to U}$) provides deeper insight into the cooperative effect of the mutational perturbation and long-range communication in the B-to-A direction. For the CNB-A domain, a $\Delta G^{\ddagger}_{F\to U}$ of 20.5 k_BT is obtained for the R333K mutant versus 18.4 k_BT for the wild-type protein. A $\Delta G^{\ddagger}_{F\to U} = 23.9$ k_BT is observed for mutant CNB-B domain versus 33.7 k_BT for the wild-type protein. The difference of 3 k_BT between the two CNB domains in the R333K mutant versus 15.3 k_BT in the wild-type protein shows that the two CNB domains in the mutant regulatory subunit have been significantly decoupled, but residual cooperativity still exists between them. These results show that the cooperativity between the two CNB domains in the PKA complex is robust and likely involves multiple residues or structural elements in the regulatory subunit.

Discussion

Accessing Microstates in the PKA Inactive State Ensemble. The CNB domains bound to the catalytic subunit displayed complex behavior, unfolding in two clearly distinct pathways. The predominant pathway (unfolding pathway I) shows that the two CNB domains are very stable and tightly coupled, unfolding nearly simultaneously, whereas the minor pathway (unfolding pathway II) resembles the apo state in which the CNB domains unfold sequentially and independently of each other. While the optical tweezers experiment directly and selectively probes the regulatory subunit, it is possible that the two unfolding pathways identified in this study may be influenced by dynamic fluctuations of the catalytic subunit (33).

The observation that the CNB domains unfold in two pathways likely represents two distinct conformations of the wild-type PKA inactive state ensemble (Fig. 4, green box). We find, in addition, that the R333K mutation promoted a greater population of loosely bound conformations (Fig. 4, tan box). In fact, no residual kinase activity of the catalytic subunit bound to the regulatory subunit cross-linked to DNA handles was detected in the absence of cAMP, indicating that complete inhibition is achieved independently of the inactive conformational state of

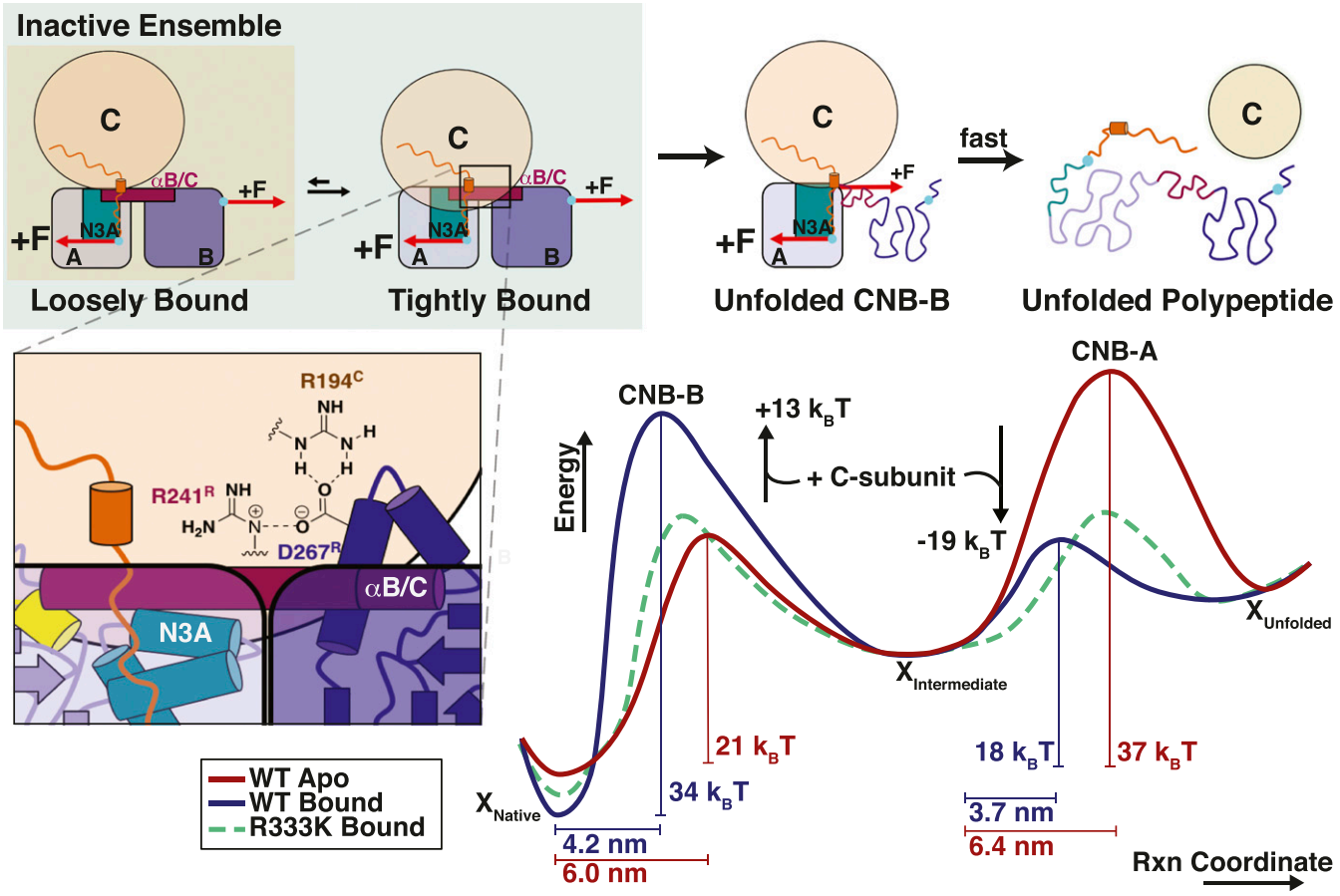

Fig. 4. A switch in the folding-energy landscape of the CNB domains controls the activation of PKA. (*Upper*) An ensemble is observed for the PKA complex in the inactive state (green box), in which the CNB-B domain exists in a tightly and a loosely bound conformation. The R333K mutation shifts the inactive ensemble toward a greater fraction of the loosely bound conformation (tan box). In the unfolding pathway, the CNB-B domain unfolds first because a greater degree of surface contacts exists between the CNB-A domain and the catalytic subunit via the N3A motif (shown in teal) and the αB/C helix (shown in maroon). The unfolding of the CNB-B domain results in the loss of the Arg241$^{(R)}$:Asp267$^{(R)}$:Arg194$^{(C)}$ salt bridge (*Enlarged View*) (41), which exposes a weaker unfolding point, or Achilles heel unfolding point, and the fast dissociation of the CNB-A domain from the catalytic subunit. (*Lower*) This cooperative unfolding pathway is also observed in the energetics of the unfolding free-energy landscape. In the absence of the catalytic subunit (apo state, red trace), a lower energy barrier is required to unfold the CNB-B domain (21 k_BT) than the CNB-A domain (37 k_BT). In contrast, in the tightly bound conformation (blue trace) a higher energy barrier is required to unfold the CNB-B domain (34 k_BT) than the CNB-A domain (18 k_BT). This change in energy barriers results in highly cooperative unfolding behavior between the two CNB domains bound to the catalytic subunit. A destabilizing mutation in the CNB-B domain (R333K, dashed green trace) partially decouples the cooperativity between the two CNB domains bound to the catalytic subunit. The energy difference in the folded state (X_{Native}) is not to scale to better distinguish the differences between the energy barriers for the apo, wild-type, and R333K protein constructs.

the PKA heterodimer (*SI Appendix*, Fig. S1). This result indicates that in both inactive conformations, reflected by unfolding pathways I and II, the regulatory subunit remains tethered to the catalytic subunit active site through the inhibitory sequence motif (34, 35). Therefore, in the predominant conformation reflected by unfolding pathway I, the inhibition of kinase activity involves interactions with the inhibitory sequence and surface interactions between the regulatory and catalytic subunits, i.e., a tightly bound conformation. In contrast, we propose that in the inactive conformation reflected in unfolding pathway II kinase inhibition is largely mediated by the inhibitory sequence without strong surface interactions between the regulatory and catalytic subunits, i.e., a loosely bound conformation. This partial dissociation of the PKA complex has been observed in bulk studies (35–37), but future experiments will be required to further characterize this secondary unfolding pathway.

The structural origin for a tightly and a loosely bound conformation may arise from the dynamics associated with the α-helix, the B/C helix, that connects the two CNB domains in the regulatory subunit (21, 36, 38). As seen in the PKA structure (Fig. 1*B*) (4), the extended conformation of the B/C helix facilitates multiple points of interaction between the regulatory and catalytic subunits. These points of interaction include the B/C helix itself, the flexible linker domain, and the two CNB domains. Therefore, the tightly bound conformation identified in this study may correspond to the regulatory subunit with the B/C helix in an extended conformation that has been previously observed in bulk studies (21).

In contrast, the loosely bound conformation suggests fewer interaction points between the regulatory and catalytic subunits. A recent study using molecular dynamic simulations has proposed that the regulatory subunit samples a flipback conformation (39) in which the B/C helix bends at residue G235 and the CNB-B domain decreases its surface interaction with the catalytic subunit. Because our results show very strong cooperativity between the two CNB domains, it is possible that breaking the interaction between the catalytic subunit and the CNB-B domain will lower the interaction energy with the CNB-A domain as well. Thus, the loosely bound conformation identified in this study may correspond to a regulatory subunit with a bent B/C helix as reported in the flipback conformation (33).

Structural Origin for the Cooperative Unfolding Mechanism of the Regulatory Subunit Bound to the Catalytic Subunit. Although the unfolding order of the CNB domains is the same in the presence and absence of the catalytic subunit, the sequence of events emerges from very different underlying energy landscapes.

In the apo state, the CNB domains behave as two independent, noninteracting structural elements, of which the CNB-B domain is the mechanically weaker domain, unfolding almost exclusively before the CNB-A domain. The strong bias in the order of unfolding events is not apparent from the small difference in unfolding force between the two CNB domains (Fig. 2). Instead, the underlying energy-landscape parameters ($\tau_{0,F}$, $\Delta x^{\ddagger}_{F\rightarrow U}$, $\Delta G^{\ddagger}_{F\rightarrow U}$) of the two domains, which result in very narrow unfolding force distributions, dictate the observed unfolding reaction order. We use Monte Carlo simulations to show that the energy–landscape parameters of each individual CNB domain fully recapitulate our experimental observations obtained with the regulatory subunit (*SI Appendix*, Fig. S3).

In contrast, in the presence of the catalytic subunit, the CNB domains unfold nearly simultaneously and in a cooperative fashion, which arises from intersubunit coupling interactions. This cooperativity between domains can be rationalized by the contacts between amino acid residues in the regulatory and catalytic subunits. In the PKA complex, the CNB-A domain has the greatest degree of surface contacts with the catalytic subunit via its N3A motif, the cAMP-binding pocket, and the flexible linker. A surface analysis of the PKA complex (4) shows that the N3A motif contributes 56% of the surface contacts between the CNB-A domain and the catalytic subunit. Additionally, the B/C helix that connects the two CNB domains contributes 26% of the total surface contacts with the catalytic subunit. In contrast, fewer contact points exist between the CNB-B domain and the catalytic subunit (Fig. 4, enlarged *Inset*), which occur mainly via a set of hydrogen bonds and electrostatic interactions between $Arg241^{(R)}$:$Asp267^{(R)}$:$Arg194^{(C)}$ and a hydrophobic stack between $Trp260^{(R)}$:$Lys285^{(C)}$:$Asn283^{(C)}$ (the superscript denotes the PKA subunit) (4). These contact points have been shown to be critical for the stability of the PKA complex; i.e., mutations in these residues facilitate the dissociation of the regulatory subunit from the catalytic subunit (40).

From our studies, we propose that a mechanical force breaks the contact points between residues in the CNB-B domain and the catalytic subunit and facilities the fast dissociation and unfolding of the CNB-A domain as shown in the schematic in Fig. 4. When unfolding the regulatory subunit, the CNB-B domain unfolds first because it has fewer surface contacts with the catalytic subunit than the CNB-A domain (18% and 42%, respectively), making the CNB-B domain the weaker of the two domains. The unfolding of CNB-B results in the loss of the $Arg241^{(R)}$:$Asp267^{(R)}$:$Arg194^{(C)}$ salt bridge and the $Trp260^{(R)}$:$Lys285^{(C)}$:$Asn283^{(C)}$ hydrophobic patch (4, 41), creating a new, weaker unfolding point, an Achilles heel that results in the fast dissociation of the CNB-A domain from the catalytic subunit (Fig. 4, *Upper Center*). This Achilles heel point may be linked to the cAMP-mediated activation of the PKA complex. In our studies, the mechanical unfolding of the CNB-B gains access to a lower unfolding-energy barrier for the fast dissociation of the PKA complex. This may be the foundation by which cAMP binding to the CNB-B domain triggers the fast release of the active catalytic subunit.

An Energetic Switch Mechanism Controls the Activation of PKA. Previous biochemical studies have shown that the cAMP-dependent activation of the PKA complex is sequential and cooperative, wherein binding of a first cAMP molecule to the CNB-B domain allows the binding of a second cAMP molecule to the CNB-A domain (8, 9). The gatekeeper role that the CNB-B domain plays in the activation pathway of PKA has been well established experimentally (4, 42, 43) and serves as a prototype example to study the thermodynamic driving forces underlying signal transduction between signaling modules, such as CNB domains.

Here, we discuss the differences in energy landscapes between the apo and bound states and their role in the mechanism of activation of PKA. Having determined the energy barriers ($\Delta G^{\ddagger}_{F\rightarrow U}$) and the unfolding reaction order of the CNB domains, we constructed an energy landscape of the regulatory subunit in the apo state and in the tightly bound conformation with the catalytic subunit (Fig. 4). Interestingly, while the unfolding reaction order of the apo state and the tightly bound conformation are the same (i.e., the CNB-B domain always unfolds first), the energy barriers underlying these two unfolding pathways are very different. For the CNB-B domain, a significantly higher energy barrier from 20.9 k_BT in the apo state to 33.5 k_BT in the tightly bound conformation is observed ($\Delta\Delta G^{\ddagger}_{F\rightarrow U}$ = 12.6 k_BT), whereas a lower energy barrier is observed for the CNB-A domain when bound to the catalytic subunit compared with the apo state ($\Delta\Delta G^{\ddagger}_{F\rightarrow U}$ = 18.2 k_BT). This switch in energy barriers triggered by the catalytic subunit results in strong cooperative interactions between the CNB domains in the B-to-A direction and provides a thermodynamic basis for the gatekeeper function of the CNB-B domain, i.e., an energetic perturbation in the CNB-B domain (mutation or ligand binding) will propagate efficiently to the CNB-A domain.

In fact, the R333K mutation shows that the unfolding forces are lower for both CNB domains compared with the wild-type regulatory subunit, despite the mutation being localized in the CNB-B domain. This result clearly shows that the destabilizing mutational effect of R333K was transduced in the B-to-A direction. In agreement with this result, analysis of the energy barriers reveals that both CNB domains remain coupled in the B-to-A direction but to a significantly lower degree than with the wild-type regulatory subunit (Fig. 4, dashed green line). It is possible that the larger cAMP concentration required to activate the PKA complex harboring R333K is due not only to a lower affinity between cAMP and the binding pocket of the mutant CNB-B domain but also to the two CNB domains being thermodynamically almost decoupled. As a consequence, the observed lack of functional cooperativity in the activation of a PKA heterotetramer harboring the R333K mutations (9) results from two mechanisms: ligand-binding defects and the inability of the CNB-B domain to efficiently transduce the cAMP-binding signal to the CNB-A domain. It is possible that disease mutations in the PKA-RIα that generate gain of function or loss of function are a consequence of an increase or decrease in the degree of thermodynamic coupling between the CNB domains (5, 41).

Conclusion

In this study, we developed a single-molecule mechanical assay based on optical tweezers to study the folding cooperativity of the CNB domains of PKA in the apo state or bound to the catalytic subunit. This approach directly interrogates the thermodynamic driving forces that enable PKA to be an effective molecular switch that transduces cAMP-binding signals from one CNB domain to another to release active catalytic subunits. Future studies will involve investigating the communication mechanisms between CNB domains across the PKA heterotetramer as well as the roles of ATP, Mg^{2+}, and the inhibitory sequence on the cooperative behavior of the CNB domains. Our approach should be readily applicable to address these fundamental questions in PKA as well as in other kinases such as PKG or PKC that share a similar structural organization.

Materials and Methods

Regulatory Subunit (RIα 71–379) Mutagenesis, Expression, and Purification. The *Bos taurus* regulatory subunit PRSET plasmid was expressed and purified using previously published established protocols (38). Briefly, all regulatory subunit constructs were expressed in BL21(DE3) pLysS-competent cells overnight at 18 °C with 1 mM isopropyl β-D-1-thiogalactopyranoside (IPTG). Cells were lysed in lysis buffer (20 mM MES, 100 mM NaCl, 2 mM EGTA, 2 mM EDTA, 5 mM DTT, pH 6.5), and the spun supernatant was precipitated with 45% ammonium

sulfate before binding to a homemade cAMP-coupled agarose resin. The protein was eluted from the resin with cGMP and was run on a size-exclusion column before attachment of the DNA handles (*SI Appendix, Section 1.1*).

Catalytic Subunit Expression and Purification. The catalytic subunit was expressed in *Escherichia coli* Rosetta (DE3)-competent cells overnight at 18 °C with 0.5 mM IPTG. The cells were lysed in lysis buffer (20 mM imidazole, 30 mM MES 50 mM KCl, 1 mM EDTA, and 5 mM DTT, pH 6.5), and the catalytic subunit was isolated using nickel agarose resin (*SI Appendix, Section 1.2*).

Attachment of DNA Handles. DNA handles were attached to the regulatory subunit using the protocol published by Hao et al. (44) to form the DNA–protein chimera. Before the 350-bp DNA handles were ligated with digoxigenin and biotin modification, the DNA–protein chimera was subjected to additional purification with a homemade cAMP-coupled agarose resin to select for functional molecules (*SI Appendix, Section 1.4*).

Kinase Activity Assay. The DNA–protein chimera was incubated with the catalytic subunit in PKA buffer (10 mM MOPS, 50 m NaCl, 1 mM $MgCl_2$, 0.2 mM ATP, pH 7.0) for 5 min on ice. Kinase inhibition or activity was tested using the PepTag Non-Radioactive Protein Kinase Assay Kit (Promega). The DNA–protein chimera and the catalytic subunit were incubated with the fluorescent Kemptide substrate in the absence and presence of cAMP. The samples were loaded onto a 0.8% agarose gel and separated by gel electrophoresis (*SI Appendix, Section 1.5* and Fig. S1).

Optical Tweezers Assay. The microfluidic chamber was equilibrated with 100 nM of freshly filtered (0.2-μm pore size) catalytic subunit in PKA buffer. The DNA–protein chimera was incubated with the catalytic subunit (100 nM) for 5 min before incubation with anti-digoxigenin (AD) beads for 30 min. After incubation, the DNA–protein and AD bead mixture was diluted with 1 mL of PKA buffer (1:1,000 dilution) before injection into the microfluidic chamber. The regulatory subunit with DNA handles was tethered between two polystyrene beads, and the formation of the PKA complex was monitored by an increase in the force and the observed cooperative unfolding pathway (*SI Appendix, Section 1.6*). For the catalytic subunit titration, ∼100–400 traces were collected from three to six different molecules for each protein concentration.

CD and Fluorescence Unfolding Experiments. Bulk urea unfolding experiments were monitored by changes in CD and tryptophan fluorescence signals using the protocols shown by Herberg et al. (9) (*SI Appendix, Section 1.7*).

ACKNOWLEDGMENTS. We thank Olga Dudko, Elizabeth Komives, Maria Fe Lanfranco, and members of the R.A.M. and S.S.T. laboratories for constructive discussions on the manuscript. This work was supported by the Clare Boothe Luce Foundation (J.P.E.), National Science Foundation Grant MCB1715572 (to R.A.M.), NIH Grants R01GM034921 (to S.S.T.) and R00CA187565 (to H.C.H.), Cancer Prevention & Research Institute of Texas Grant RR170036 (to H.C.H.), and Gabrielle's Angel Foundation for Cancer Research (H.C.H.).

1. Taylor SS, Ilouz R, Zhang P, Kornev AP (2012) Assembly of allosteric macromolecular switches: Lessons from PKA. *Nat Rev Mol Cell Biol* 13:646–658.
2. Nussinov R, Tsai C-J (2013) Allostery in disease and in drug discovery. *Cell* 153:293–305.
3. Taylor SS, et al. (2008) Signaling through cAMP and cAMP-dependent protein kinase: Diverse strategies for drug design. *Biochim Biophys Acta* 1784:16–26.
4. Kim C, Cheng CY, Saldanha SA, Taylor SS (2007) PKA-I holoenzyme structure reveals a mechanism for cAMP-dependent activation. *Cell* 130:1032–1043.
5. Bruystens JGH, et al. (2014) PKA RIα homodimer structure reveals an intermolecular interface with implications for cooperative cAMP binding and Carney complex disease. *Structure* 22:59–69.
6. Kim C, Xuong N-H, Taylor SS (2005) Crystal structure of a complex between the catalytic and regulatory (RIalpha) subunits of PKA. *Science* 307:690–696.
7. McNicholl ET, Das R, SilDas S, Taylor SS, Melacini G (2010) Communication between tandem cAMP binding domains in the regulatory subunit of protein kinase A-Ialpha as revealed by domain-silencing mutations. *J Biol Chem* 285:15523–15537.
8. Herberg FW, Dostmann WR, Zorn M, Davis SJ, Taylor SS (1994) Crosstalk between domains in the regulatory subunit of cAMP-dependent protein kinase: Influence of amino terminus on cAMP binding and holoenzyme formation. *Biochemistry* 33: 7485–7494.
9. Herberg FW, Taylor SS, Dostmann WR (1996) Active site mutations define the pathway for the cooperative activation of cAMP-dependent protein kinase. *Biochemistry* 35:2934–2942.
10. Boettcher AJ, et al. (2011) Realizing the allosteric potential of the tetrameric protein kinase A RIα holoenzyme. *Structure* 19:265–276.
11. Das R, et al. (2007) cAMP activation of PKA defines an ancient signaling mechanism. *Proc Natl Acad Sci USA* 104:93–98.
12. Boras BW, Kornev A, Taylor SS, McCulloch AD (2014) Using Markov state models to develop a mechanistic understanding of protein kinase A regulatory subunit RIα activation in response to cAMP binding. *J Biol Chem* 289:30040–30051.
13. Neuman KC, Nagy A (2008) Single-molecule force spectroscopy: Optical tweezers, magnetic tweezers and atomic force microscopy. *Nat Methods* 5:491–505.
14. Cecconi C, Shank EA, Marqusee S, Bustamante C (2011) DNA molecular handles for single-molecule protein-folding studies by optical tweezers. *Methods Mol Biol* 749: 255–271.
15. Zhang Y (2017) Energetics, kinetics, and pathway of SNARE folding and assembly revealed by optical tweezers. *Protein Sci* 26:1252–1265.
16. Zhang X, Ma L, Zhang Y (2013) High-resolution optical tweezers for single-molecule manipulation. *Yale J Biol Med* 86:367–383.
17. Cecconi C, Shank EA, Bustamante C, Marqusee S (2005) Direct observation of the three-state folding of a single protein molecule. *Science* 309:2057–2060.
18. Shank EA, Cecconi C, Dill JW, Marqusee S, Bustamante C (2010) The folding cooperativity of a protein is controlled by its chain topology. *Nature* 465:637–640.
19. Kaiser CM, Goldman DH, Chodera JD, Tinoco I, Jr, Bustamante C (2011) The ribosome modulates nascent protein folding. *Science* 334:1723–1727.
20. Durgerian S, Taylor SS (1989) The consequences of introducing an autophosphorylation site into the type I regulatory subunit of cAMP-dependent protein kinase. *J Biol Chem* 264:9807–9813.
21. Cheng CY, Yang J, Taylor SS, Blumenthal DK (2009) Sensing domain dynamics in protein kinase A-Ialpha complexes by solution X-ray scattering. *J Biol Chem* 284: 35916–35925.
22. Herberg FW, Taylor SS (1993) Physiological inhibitors of the catalytic subunit of cAMP-dependent protein kinase: Effect of MgATP on protein-protein interactions. *Biochemistry* 32:14015–14022.
23. Bustamante C, Marko JF, Siggia ED, Smith S (1994) Entropic elasticity of lambda-phage DNA. *Science* 265:1599–1600.
24. Dudko OK, Hummer G, Szabo A (2008) Theory, analysis, and interpretation of single-molecule force spectroscopy experiments. *Proc Natl Acad Sci USA* 105:15755–15760.
25. Dudko OK, Hummer G, Szabo A (2006) Intrinsic rates and activation free energies from single-molecule pulling experiments. *Phys Rev Lett* 96:108101.
26. Bustamante C, Chemla YR, Forde NR, Izhaky D (2004) Mechanical processes in biochemistry. *Annu Rev Biochem* 73:705–748.
27. Brockwell DJ, et al. (2003) Pulling geometry defines the mechanical resistance of a β-sheet protein. *Nat Struct Biol* 10:731–737.
28. Williams PM, et al. (2003) Hidden complexity in the mechanical properties of titin. *Nature* 422:446–449.
29. Brockwell DJ, et al. (2005) Mechanically unfolding the small, topologically simple protein L. *Biophys J* 89:506–519.
30. Dietz H, Berkemeier F, Bertz M, Rief M (2006) Anisotropic deformation response of single protein molecules. *Proc Natl Acad Sci USA* 103:12724–12728.
31. Elms PJ, Chodera JD, Bustamante C, Marqusee S (2012) The molten globule state is unusually deformable under mechanical force. *Proc Natl Acad Sci USA* 109:3796–3801.
32. Cànaves JM, Leon DA, Taylor SS (2000) Consequences of cAMP-binding site mutations on the structural stability of the type I regulatory subunit of cAMP-dependent protein kinase. *Biochemistry* 39:15022–15031.
33. Sims PC, et al. (2013) Electronic measurements of single-molecule catalysis by cAMP-dependent protein kinase A. *J Am Chem Soc* 135:7861–7868.
34. Akimoto M, et al. (2013) Signaling through dynamic linkers as revealed by PKA. *Proc Natl Acad Sci USA* 110:14231–14236.
35. Vigil D, et al. (2004) Conformational differences among solution structures of the type Ialpha, IIalpha and IIbeta protein kinase A regulatory subunit homodimers: Role of the linker regions. *J Mol Biol* 337:1183–1194.
36. Gullingsrud J, Kim C, Taylor SS, McCammon JA (2006) Dynamic binding of PKA regulatory subunit RI alpha. *Structure* 14:141–149.
37. Wu J, Jones JM, Nguyen-Huu X, Ten Eyck LF, Taylor SS (2004) Crystal structures of RIalpha subunit of cyclic adenosine 5′-monophosphate (cAMP)-dependent protein kinase complexed with (Rp)-adenosine 3′,5′-cyclic monophosphothioate and (Sp)-adenosine 3′,5′-cyclic monophosphothioate, the phosphothioate analogues of cAMP. *Biochemistry* 43:6620–6629.
38. Taylor SS, et al. (2004) PKA: A portrait of protein kinase dynamics. *Biochim Biophys Acta* 1697:259–269.
39. Hirakis SP, Malmstrom RD, Amaro RE (2017) Molecular simulations reveal an unresolved conformation of the type IA protein kinase A regulatory subunit and suggest its role in the cAMP regulatory mechanism. *Biochemistry* 56:3885–3888.
40. Barros EP, et al. (2017) Electrostatic interactions as mediators in the allosteric activation of protein kinase A RIα. *Biochemistry* 56:1536–1545.
41. Bruystens JG, et al. (2016) Structure of a PKA RIα recurrent acrodysostosis mutant explains defective cAMP-dependent activation. *J Mol Biol* 428:4890–4904.
42. Moorthy BS, Badireddy S, Anand GS (2011) Cooperativity and allostery in cAMP-dependent activation of protein kinase A: Monitoring conformations of intermediates by amide hydrogen/deuterium exchange. *Int J Mass Spectrom* 302:157–166.
43. Krishnamurthy S, Tulsian NK, Chandramohan A, Anand GS (2015) Parallel allostery by cAMP and PDE coordinates activation and termination phases in cAMP signaling. *Biophys J* 109:1251–1263.
44. Hao Y, Canavan C, Taylor SS, Maillard RA (2017) Integrated method to attach DNA handles and functionally select proteins to study folding and protein-ligand interactions with optical tweezers. *Sci Rep* 7:10843.